

Uncoupling electrokinetic flow solutions

Kristopher L. Kuhlman · Bwalya Malama

Abstract The continuum-scale electrokinetic porous-media flow and excess charge redistribution equations are uncoupled using eigenvalue decomposition. The uncoupling results in a pair of independent diffusion equations for “intermediate” potentials subject to modified material properties and boundary conditions. The fluid pressure and electrostatic potential are then found by recombining the solutions to the two intermediate uncoupled problems in a matrix-vector multiply. Expressions for the material properties or source terms in the intermediate uncoupled problem may require extended precision or careful re-writing to avoid numerical cancellation, but the solutions themselves can be computed in typical double precision. The approach works with analytical or gridded numerical solutions and is illustrated through two examples. The solution for flow to a pumping well is manipulated to predict streaming potential and electroosmosis, and a periodic one-dimensional analytical solution is derived and used to predict electroosmosis and streaming potential in a laboratory flow cell subjected to low frequency alternating current and pressure excitation. The examples illustrate the utility of the eigenvalue decoupling approach, repurposing existing analytical solutions and leveraging simpler-to-derive solutions or numerical models for coupled physics.

Keywords streaming potential · electroosmosis · electrokinetic · eigenvalue · coupled processes · geophysics

K.L. Kuhlman
Sandia National Laboratories
Applied Systems Analysis and Research Department
Albuquerque, NM
E-mail: klkuhlm@sandia.gov

B. Malama
California Polytechnic State University, San Luis Obispo
Natural Resources Management & Environmental Sciences
San Luis Obispo, CA
E-mail: bmalama@calpoly.edu

1 Introduction

Coupled physical phenomena exist at the intersection of hydrological and geophysical processes, and advanced solution methods are required to make general predictions. Radioactive waste disposal (Tsang et al. 2012), water resource management (Barthel and Banzhaf 2016), geothermal energy production (Bächler and Kohl 2005), and hydrogeophysics (Hinnell et al. 2010) are examples of applications requiring holistic approaches to multiphysics. Although several alternative commercial (Li et al. 2009) and research (Guyer et al. 2009, Gaston et al. 2009, Liu 2013) software libraries exist to solve coupled physics using finite element or finite volume numerical methods, we illustrate an approach allowing adaptation of existing analytical or numerical methods when certain symmetries exist in the governing equations and boundary conditions. Coupled analytical solutions derived using this approach may serve to validate solutions obtained with traditional numerical methods.

While many exploration geophysical methods are sensitive to the presence or storage of water or solutes (e.g., electrical resistivity (Pollock and Cirkpa 2012), seismic (Hyndman et al. 1994), or induced polarization (Ahmed et al. 2019)), in electrokinetics the coupling between hydrology and geophysics is especially explicit and direct (Revil and Jardani 2013, Revil et al. 2015). Direct causality exists between processes of flow and electric potentials for streaming potentials and electrokinetics. Streaming potentials are caused by the movement of water through a porous medium and electroosmosis is the movement water in low-permeability porous media due to applied electric fields. Electrokinetics occur when electrolytes (e.g., water and ions) flow through a porous medium with a surface charge (e.g., quartz sand grains) (Pride 1994, Bockris and Reddy 2002). Streaming potentials arise from the movement of water under an imposed pressure gradient, dragging ions with the water, creating a streaming current. Electroosmotic pressure arises from the movement of ions under an imposed electric field, dragging the water with the ions, creating an electroosmotic flux. Here, we account for both coupled electrokinetic processes occurring in a porous medium by decoupling the two governing equations and boundary conditions, solving for intermediate potentials, and recombining to get back the physical solution. The approach relies on transient effects in both of the governing equations, boundary conditions of the same type at each location in the electrical and hydrological problems, and equivalent anisotropy in the material properties of the electrical and hydrologic problems.

Streaming potentials are useful at both the laboratory and field scales to characterize water movement using passive (i.e., self-potential without an applied current) voltage observations (Revil and Jardani 2013, Revil 2017). Streaming potentials have been used to derive material properties from field-scale pumping tests experiments (Revil et al. 2008, Malama et al. 2009b;a, Malama 2014, Soueid Ahmed et al. 2016). Electroosmosis is utilized widely in microfluidics (Karniadakis et al. 2005) and at the pore scale (Coelho et al. 1996, Gupta et al. 2008) to move fluids through small pores. At the laboratory and field scale it has been used to consolidate soft clays (Banerjee and Mitchell 1980, Banerjee and Vitayasupakorn 1984, Lo et al. 1991, Alshawabkeh et al. 2004) or mobilize contaminants (Bruell et al. 1992, Acar et al. 1993, Shapiro and Probstein 1993, Acar and Alshawabkeh 1996, Virkutyte et al. 2002, Bertolini et al.

2009). Seismoelectric applications consider the electrokinetic response of a porous formation to seismic waves (Pride 1994, Haines and Pride 2006, Revil et al. 2015, Peng et al. 2019).

Predictions of streaming potentials and electroosmosis responses can be made using analytical solutions, but typically these solutions are one-way coupled (i.e., only explicitly accounting for one of the two conjugate electrokinetic effects). For example, typical streaming potential solutions use the existing solution for flow to a well (ignoring electroosmotic effects) as a source term in the electrical conduction equation (Malama et al. 2009a;b, Malama 2014). A typical electroosmosis solution uses the existing solutions for electrical conduction around an electrode (ignoring streaming potential effects) as a source term in the flow equation (Banerjee and Mitchell 1980, Shapiro and Probstein 1993, Reppert and Morgan 2002). Few fully coupled porous-media scale electrokinetic solutions exist; Pengra et al. (1999) showed under simplified laboratory conditions independent measurement of electroosmotic pressure and streaming potentials can be used to estimate the permeability of porous materials. More general predictions of fully coupled electrokinetics are usually done with finite-element or finite-volume multiphysics solution libraries like COMSOL or OpenFOAM (Probstein 1994, Masliyah and Bhattacharjee 2006, Revil et al. 2015).

Electrokinetic flow through porous media is presented here in a matrix formulation, with the two equations decoupled using an eigenvalue decomposition. The uncoupled solutions are two simpler diffusion equation solutions that can more readily be solved using analytical solutions or existing numerical models; solutions to these intermediate solutions are then recombined to solve the original electrokinetic problem. The approach should be applicable to coupling of constitutive laws including Darcy's law (porous media flow), Fourier's law (heat conduction), and Ohm's law (charge conduction) because the system of coupled equations can be represented as a symmetric system of equations, because these types of processes lead to the required types of symmetric equations.

While an analogous uncoupling approach has been used in quantum mechanics for second-order inelastic scattering equations (Stechel et al. 1978, Light et al. 1979) and in geophysics to decouple poroelastic and acoustic wave equations (Lo et al. 2009), the method has not previously been applied to uncouple electrokinetic phenomena. The authors were inspired for this approach by the eigenvalue approach to uncoupling a multilayered aquifer and aquitard flow system found in publications by Maas and Hemker (Hemker 1984, Maas 1986; 1987). Following the analogy with the layered aquifer system, the coupled equations in matrix form could also be solved directly using special functions of matrix argument (Maas 1986).

In Section 2 we present the governing equations for electrokinetic flow and rewrite them in dimensionless form. Section 3 presents the uncoupling process for both the governing equations and boundary conditions. Section 4 shows two examples. The first example (Section 4.1) uses type-curve methods to represent electrokinetic flow to a well, and the second example (Section 4.2) predicts the response of a laboratory sample to periodic pressure and electrical excitation. Finally, we summarize the capabilities and limitations of the approach (Section 5).

2 Electrokinetic Governing Equations

The decoupling approach relies on symmetry in the governing equations and boundary conditions. We begin with expressions for the Darcy and electric current densities (i.e., fluxes) in terms of potential gradients (i.e., thermodynamic forces)

$$\begin{aligned} \mathbf{j}_e &= -\sigma_0 \nabla \psi - L_{12} \nabla p \\ \mathbf{j}_f &= -L_{21} \nabla \psi - \frac{k_0}{\mu} \nabla p \end{aligned} \quad (1)$$

where \mathbf{j}_e and \mathbf{j}_f are electrical [A/m^2] and Darcy (i.e., fluid-volume) [m/sec] current densities, σ_0 is bulk electrical conductivity [S/m], k_0 is porous medium intrinsic permeability [m^2], μ is pore water dynamic viscosity [$Pa \cdot sec$], $\{L_{12}, L_{21}\}$ are porous medium electrokinetic coupling coefficients [$A/m \cdot Pa$], [$m^2/V \cdot sec$], ψ is change in electrostatic potential [V] (in the quasi-static limit with no magnetic sources), and p is change in liquid pressure [Pa]. Both p and ψ are changes from an arbitrary initial state due to some forcing (e.g., pumping or recharge). The zero subscripts on k and σ differentiate them from similar quantities (i.e., $\mathbf{j}_{Darcy} = -k/\mu \nabla p$ or $\mathbf{j}_{Ohm} = -\sigma \nabla \psi$) that do not consider electrokinetic coupling effects (Pengra et al. 1999).

Revil and Jardani (2013) present the streaming potential coupling coefficient in terms of pore-scale electrokinetic quantities (Bockris and Reddy 2002) as

$$L_{12} = \frac{\varepsilon \zeta \sigma_0}{\mu (\sigma_f + F \sigma_s)} \quad (2)$$

where ε is the pore-fluid dielectric constant [F/m], ζ is the zeta potential at the pore/fluid interface [V], σ_f and σ_s are the electrical conductivity of the individual fluid and solid components, and F is the dimensionless formation factor, defined as the resistivity of the fluid-saturated rock normalized by the pore fluid resistivity. In the geotechnical literature, L_{21} is electroosmotic permeability (k_e) with a similar definition in terms of pore-scale quantities (Casagrande 1949, Arnold 1973).

Mass and charge conservation expressions are conveniently and symmetrically written in terms of flux divergence as

$$\begin{aligned} -\nabla \cdot \mathbf{j}_e &= C^* \frac{\partial \psi}{\partial t} \\ -\nabla \cdot \mathbf{j}_f &= nc \frac{\partial p}{\partial t}, \end{aligned} \quad (3)$$

where n is dimensionless porosity, c is compressibility [$1/Pa$], and C^* is specific capacitance [$C/(m^3 \cdot V)$], that is electrolyte charge flowing into a unit volume per unit change in potential (Corapcioglu 1991). Typically, in streaming potential problems $\nabla \cdot \mathbf{j}_e = 0$ (Revil and Jardani 2013), but without loss of generality we include a small transient capacitance term to maintain symmetry in the governing equations required by the uncoupling approach.

Substituting the fluxes (1) into the conservation equations (3) leads to two coupled differential equations in terms of potentials,

$$\begin{aligned} C^* \frac{\partial \psi}{\partial t} &= \nabla \cdot (\sigma_0 \nabla \psi) + \nabla \cdot (L_{12} \nabla p) \\ nc \frac{\partial p}{\partial t} &= \nabla \cdot (L_{21} \nabla \psi) + \nabla \cdot \left(\frac{k_0}{\mu} \nabla p \right). \end{aligned} \quad (4)$$

These coupled equations can be written as a matrix differential equation. In the derivation we assume σ_0 , k_0 , μ , L_{12} , and L_{21} are piecewise constant in space (allowing them to be taken outside the divergence operator), which results in the form

$$\begin{bmatrix} C^* & 0 \\ 0 & nc \end{bmatrix} \frac{\partial}{\partial t} \begin{bmatrix} \psi \\ p \end{bmatrix} = \begin{bmatrix} \sigma_0 & L_{12} \\ L_{21} & \frac{k_0}{\mu} \end{bmatrix} \nabla^2 \begin{bmatrix} \psi \\ p \end{bmatrix}. \quad (5)$$

The approach requires assumption of piecewise constancy in material parameters which can violate flux continuity at property discontinuities in numerical models with linear interpolation functions, but still allows either layers or regions of different material properties. The limitations of the approach are summarized in Section 5.

This can be additionally re-arranged, pre-multiplying by the diagonal storage properties matrix inverse, leaving

$$\frac{\partial \mathbf{d}}{\partial t} = \begin{bmatrix} \alpha_E & \alpha_E K_S \\ \alpha_H K_E & \alpha_H \end{bmatrix} \nabla^2 \mathbf{d}, \quad (6)$$

where $\mathbf{d} = [\psi, p]^T$ is the physical potential vector, $\alpha_H = k_0/(\mu nc)$ is the hydraulic diffusivity [m^2/sec], $\alpha_E = \sigma_0/C^*$ is the electrostatic potential diffusivity [m^2/sec], $K_S = L_{12}/\sigma_0$ is the streaming potential [V/Pa], and $K_E = L_{21}\mu/k_0$ is the electroosmosis pressure [Pa/V].

Based on a thermodynamic argument of microscopic reversibility, Onsager (1931a;b) showed the off-diagonal coupling coefficients in expressions like (5) are symmetric ($L_{12} = L_{21}$) when the fluxes and forces are written correctly (Luikov 1975, Corapcioglu 1991). With manipulation, the dimensions of L_{12} [$\text{A}/\text{Pa} \cdot \text{m}$] and L_{21} [$\text{m}^2/\text{V} \cdot \text{sec}$] can be shown to be equivalent, indicating the equations are written in the correct form. Using this equality, we express permeability in terms of the streaming potential and the electroosmotic pressure $K_E = K_S \sigma_0 \mu / k_0$ or $k_0 = \sigma_0 \mu \frac{K_S}{K_E}$ (Pengra et al. 1999, Pengra and Wong 1999). When $L_{12} = L_{21} = 0$ the streaming potential and electroosmotic pressure cease to exist; zeroing these coefficients makes the matrix in (6) diagonal, where the flow and electrostatic problems are independent and uncoupled.

Starting with (6), we multiply the ψ equation by $L_c^2/(\alpha_H \Psi_c)$ and multiply the p equation by $L_c^2/(\alpha_H P_c)$. Characteristic electrostatic potential ($\Psi_c = P_c K_S$), pressure (P_c), time ($T_c = L_c^2/\alpha_H$), and length (L_c) are used to re-write the equations in non-dimensional form in terms of $x_D = x/L_c$, $t_D = t/T_c$, $p_D = p/P_c$, $\psi_D = \psi/\Psi_c$, and ∇_D^2 (the dimensionless Laplacian). The governing equation becomes

$$\frac{\partial \mathbf{d}_D}{\partial t} = \mathbf{A} \nabla_D^2 \mathbf{d}_D \quad (7)$$

where $\mathbf{A} = \begin{bmatrix} \alpha_D & \alpha_D \\ K_D & 1 \end{bmatrix}$ is the dimensionless matrix of Laplacian operator coefficients,

$\alpha_D = \alpha_E / \alpha_H$ is the dimensionless electrical/hydrological diffusivity ratio, $\mathbf{d}_D = [\psi / \Psi_c, p / P_c]^T$ is the dimensionless potential vector, and $K_D = K_E K_S$ is the dimensionless product of the electroosmotic pressure and streaming potential, representing the magnitude of electrokinetic coupling. In the formulation presented here these two dimensionless quantities completely characterize the electrokinetic problem, reducing the problem from four free parameters ($\alpha_H, \alpha_E, K_S, K_E$) to two. This reduction in free parameters does not limit the range of validity of the solution, it properly simplifies the previously over-constrained solution space (two equations in terms of two potentials were related with four parameters). L_c and P_c are chosen from the physical problem configuration (e.g., domain size and applied boundary or initial conditions), while T_c and Ψ_c are specified as part of re-writing the governing equations in dimensionless form (two examples of this approach are presented in Section 4). We follow a variable convention where bold lower-case are vectors and bold upper-case are matrices (see Tables 2 and 3 for notation).

3 Uncoupling

The uncoupling approach relies on decomposing the matrix characterizing the operator in the governing equation into a diagonal matrix using its eigenvalues and eigenvectors (i.e., spectral decomposition). While the approach has been used in geophysics to decouple poroelastic wave equations (Lo et al. 2009), and in quantum mechanics to uncouple second-order differential equations regarding elastic scattering (Stechel et al. 1978, Light et al. 1979), it has not previously been applied to uncoupling electrokinetic processes.

3.1 Governing Equations

The method requires \mathbf{A} is diagonalizable (i.e., it has a complete, linearly independent set of eigenvectors), so it can be decomposed into its eigenvectors and eigenvalues as $\mathbf{A} = \mathbf{S}\mathbf{\Lambda}\mathbf{S}^{-1}$ (e.g., Strang (1988, §5.2)). A non-repeating set of eigenvalues is also indicative of diagonalizability, but some cases with repeating eigenvalues may still be diagonalizable. \mathbf{S} is a matrix with the eigenvectors of \mathbf{A} as columns, and $\mathbf{\Lambda}$ is a diagonal matrix with the eigenvalues of \mathbf{A} along the diagonal, with the eigenvectors and eigenvalues in corresponding order. These are substituted into (7) and the expression is pre-multiplied by \mathbf{S}^{-1} (assuming \mathbf{S} and \mathbf{S}^{-1} are piecewise constant in space and time and can be commuted with derivatives)

$$\frac{\partial}{\partial t_D} \mathbf{S}^{-1} \mathbf{d}_D = (\mathbf{S}^{-1} \mathbf{S}) \mathbf{\Lambda} \nabla_D^2 \mathbf{S}^{-1} \mathbf{d}_D, \quad (8)$$

resulting in $\frac{\partial \boldsymbol{\delta}}{\partial t_D} = \mathbf{\Lambda} \nabla_D^2 \boldsymbol{\delta}$, where $\boldsymbol{\delta} = \mathbf{S}^{-1} \mathbf{d}_D$. This expression can be simplified because $\mathbf{S}\mathbf{S}^{-1} = \mathbf{I}$ is the identity matrix. The two equations are now uncoupled in terms of the newly defined intermediate potential $\boldsymbol{\delta}$ because $\mathbf{\Lambda}$ is a diagonal matrix.

For the 2×2 dimensionless electrokinetic problem, the eigenvectors and eigenvalues are computed from the characteristic equation to be

$$\begin{aligned} \mathbf{S} &= \begin{bmatrix} \frac{2\alpha_D}{1-\alpha_D-\Delta} - \frac{1}{2K_D}(1-\alpha_D-\Delta) & \\ 1 & 1 \end{bmatrix} \\ \mathbf{A} &= \begin{bmatrix} \frac{2\alpha_D(1-K_D)}{1+\alpha_D+\Delta} & 0 \\ 0 & \frac{1}{2}(1+\alpha_D+\Delta) \end{bmatrix} \\ \mathbf{S}^{-1} &= \frac{1}{\Delta} \begin{bmatrix} -K_D & -\frac{1}{2}(1-\alpha_D-\Delta) \\ K_D & \frac{-2K_D\alpha_D}{1-\alpha_D-\Delta} \end{bmatrix}, \end{aligned} \quad (9)$$

where

$$\Delta = \sqrt{1 + \alpha_D(4K_D - 2 + \alpha_D)}. \quad (10)$$

The uncoupled solution is computed for the two components of $\boldsymbol{\delta}$ (i.e., the intermediate potentials) then the physical solution (\mathbf{d}_D) is found from $\boldsymbol{\delta}$ via a matrix-vector multiply.

If the two differential equations for hydraulic and electrical flow were not coupled ($K_E = K_S = 0$), \mathbf{A} would already be a diagonal matrix. Writing the governing equations in the one-way coupled form (i.e., including effects of streaming potential, but not including electroosmosis – or vice-versa) results in a degenerate system of equations which cannot be decoupled using the eigenvalue approach. This one-way coupling approach, although common (Casagrande 1949, Banerjee and Mitchell 1980, Malama et al. 2009a;b) and approximately correct, is physically inconsistent. Since thermodynamics requires $L_{12} = L_{21}$, setting only one of these coefficients to zero breaks the symmetry identified by Onsager (1931a;b).

Benefitting numerical evaluation, Δ (10) will never be complex for positive α_D and K_D . For a typical aquifer $K_D \ll 1$ (i.e., $K_S \approx 10^{-8}$ [V/Pa] and $K_E \approx 10^2$ [Pa/V]; (Pengra et al. 1999)), the eigenvalues (Λ_{11} and Λ_{22}) will both be positive. The eigenvalues correspond to the permeability or hydraulic conductivity coefficients used in existing numerical hydrologic simulators. When the eigenvalues are positive existing numerical simulators (e.g., MODFLOW (Harbaugh 2005) or PFLOTRAN (Hammond et al. 2014)) can be used to solve for the intermediate potentials. The eigenvalues would be substituted for the permeability or hydraulic conductivity, while the storage coefficient or compressibility would be set to unity (depending on the details and units expected in the implementation). Physics precludes negative eigenvalues.

The forms of the uncoupled coefficients (9) are written to reduce catastrophic numerical cancellation due to subtraction of like-sized terms. If the naive quadratic formula is used (e.g., `EigenSystem[]` returned by Mathematica (Wolfram Research, Inc. 2019)), severe cancellation will occur because α_D and Δ may differ by one part in 10^{10} , rendering this difference numerically inaccurate. For example, the first eigenvalue could be equivalently written $\Lambda_{11} = \frac{1}{2}(1 + \alpha_D - \Delta)$, but this would need to be computed in quadruple-precision to get a double-precision accurate result (since $\alpha_D \approx \Delta$).

To compute p_D and ψ_D from the intermediate $\boldsymbol{\delta}$ components, pre-multiply by \mathbf{S} , $\mathbf{d}_D = \mathbf{S}\boldsymbol{\delta} = \mathbf{S}\mathbf{S}^{-1}\mathbf{d}_D$. The expression for $\boldsymbol{\delta}$ in terms of physical variables is used to

express source terms or boundary conditions from the intermediate problem in terms of the source terms or boundary conditions of the physical problem, namely

$$\boldsymbol{\delta} = \begin{bmatrix} \delta_1 \\ \delta_2 \end{bmatrix} = \frac{1}{\Delta} \begin{bmatrix} -H p_D - K_D \psi_D \\ G p_D + K_D \psi_D \end{bmatrix}, \quad (11)$$

where

$$G = \frac{-2K_D \alpha_D}{1 - \alpha_D - \Delta} \quad H = \frac{1}{2} (1 - \alpha_D - \Delta). \quad (12)$$

The expression for G has also been re-written to minimize cancellation between α_D and Δ . The physical potentials (\mathbf{d}_D) are given in terms of intermediate variables as

$$\mathbf{d}_D = \begin{bmatrix} \psi_D \\ p_D \end{bmatrix} = \begin{bmatrix} \frac{-1}{k_D} (G \delta_1 + H \delta_2) \\ \delta_1 + \delta_2 \end{bmatrix}, \quad (13)$$

which is used to compute the final physical result from the intermediate representation.

The solution procedure begins by first computing boundary conditions for the intermediate problem from the physical problem, then solving two intermediate uncoupled diffusion problems, and finally recombining the intermediate results to obtain the physical potentials. The physical properties (i.e., diffusivities) for the two intermediate problems are given by Λ_{11} and Λ_{22} (eigenvalue matrix diagonals). The boundary conditions or source terms for the intermediate potentials (i.e., in terms of $\boldsymbol{\delta}$) are determined from (11). Finally, the physical potentials are found from the intermediate potentials by a matrix-vector multiplication (13).

3.2 Boundary Conditions

To solve the intermediate differential equations, any inhomogeneous boundary and initial conditions must also be expressed in terms of $\boldsymbol{\delta}$. The most general inhomogeneous Robin (Type III) boundary condition that can be accommodated by the uncoupling approach is

$$\hat{n} \cdot d_c \nabla_D \mathbf{d}_D = n_c \mathbf{d}_D + \mathbf{c}, \quad (14)$$

where \hat{n} is the boundary normal unit vector, d_c is the dimensionless scalar Dirichlet coefficient, n_c is the dimensionless scalar Neumann coefficient, and \mathbf{c} is a dimensionless inhomogeneous constant vector. By setting either d_c or n_c to zero, an inhomogeneous Dirichlet (Type I) or Neumann (Type II) condition can be specified. By setting \mathbf{c} to zero, a homogeneous boundary condition can be specified. One equation can be homogeneous, and the other inhomogeneous, by setting only one term in \mathbf{c} to zero. Pre-multiplying through by \mathbf{S}^{-1} gives the boundary condition for the intermediate potentials in terms of $\boldsymbol{\delta}$ as

$$\hat{n} \cdot d_c \nabla_D \boldsymbol{\delta} = n_c \boldsymbol{\delta} + \boldsymbol{\gamma}, \quad (15)$$

where $\boldsymbol{\gamma} = \mathbf{S}^{-1} \mathbf{c}$ is the transformed inhomogeneous term, of the same form as (11).

3.3 Extension

This same uncoupling approach could be applied to larger systems of equation, using Cramer's rule to algebraically solve the resulting eigenvalue problem (Strang 1988). Coupled processes may include temperature, electrostatic potential, and solute concentration (Luikov 1975, Corapcioglu 1991, Leinov and Jackson 2014). The 2×2 formulation presented here could readily be extended to a 3×3 system including thermal flux and temperature gradient driving forces. Minimizing cancellation in the expressions could become much more tedious with larger systems, but automatic term re-writing software (e.g., Herbie (Panchevka et al. 2015)) could automate this. For larger coupled equation systems, the same approach should still be possible, but the uncoupling could more efficiently be done numerically (e.g., using eigenvalue and eigenvector routines in LAPACK (Anderson et al. 1990)).

4 Applications

We present two applications to demonstrate the eigenvalue uncoupling approach for electrokinetics. The first is one-dimensional cylindrically symmetric flow to a well in an infinite planar aquifer and the second is Cartesian one-dimensional flow driven by harmonic source terms on one end of a finite domain.

4.1 Streaming Potential from Pumping a Well

The application geometry is a fully penetrating line-source well in a confined aquifer with electrically insulating aquicludes (i.e., no hydraulic or electric flow) above and below. This application is not chosen for its physical realism to field streaming potential applications, but as a simple example using a well-known solution. The characteristic length is the aquifer thickness ($L_c = b$), the characteristic pressure is derived from the specified volumetric pumping rate ($P_c = \mu Q_T / (4\pi b k_0)$).

Appendix A presents the original and dimensionless form of the governing equations, boundary conditions, and initial conditions. The intermediate governing equations and initial/boundary conditions (A.22 & A.23) can be solved with the Theis (1935) solution, defined as the exponential integral of the first kind, a well-known solution for flow to a well in a confined 2D aquifer of infinite radial extent ($T \nabla^2 s = S \frac{\partial s}{\partial t}$) (Batu 1998, Lee 1999),

$$s = \frac{Q_T}{4\pi T} E_1 \left(\frac{r^2 S}{4Tt} \right), \quad (16)$$

where s is drawdown (i.e., change in hydraulic head) [m], T is transmissivity [m^2/sec], and S is the dimensionless storage coefficient (commonly referred to as storativity).

Substituting the relevant parameter definitions ($s \rightarrow \delta_i$, $T \rightarrow \Lambda_{ii}$, $S \rightarrow 1$, $Q_T \rightarrow Q_i$), the solution to the intermediate potentials can be expressed simply in the form used

Table 1 Parameters specified (left) and computed (right) for This example (six non-zero significant figures).

α_D	K_D	Δ	Λ_{11}	Λ_{22}	G	H	Q_1	Q_2
10^2	10^{-1}	99.2018	0.899093	100.101	1.00907×10^{-1}	-99.1009	1.99998	1.8291×10^{-5}
10^2	10^{-4}	99.0002	0.999899	100	1.0101×10^{-4}	-99.0001	2	2.0404×10^{-8}
10^2	10^{-7}	99	1	100	1.0101×10^{-7}	-99	2	2.04061×10^{-11}
10^5	10^{-1}	99999.2	0.899999	10^5	1.00001×10^{-1}	-99999.1	2	1.80003×10^{-11}
10^5	10^{-4}	99999	0.9999	10^5	1.00001×10^{-4}	-99999	2	1.99984×10^{-14}
10^5	10^{-7}	99999	1	10^5	1.00001×10^{-7}	-99999	2	2.00004×10^{-17}
10^8	10^{-1}	10^8	0.9	10^8	10^{-1}	-10^8	2	1.8×10^{-17}
10^8	10^{-4}	10^8	0.9999	10^8	10^{-4}	-10^8	2	1.9998×10^{-20}
10^8	10^{-7}	10^8	1	10^8	10^{-7}	-10^8	2	2×10^{-23}

in “type-curve” analysis on log-log scale plots (e.g., Batu (1998)),

$$\begin{aligned}
 \text{x axis :} & \quad \overbrace{\ln \left[\frac{t}{r^2} \right]}^{\text{data}} = \ln \left[\frac{1}{4\Lambda_{ii}} \right] + \overbrace{\ln \left[\frac{1}{u} \right]}^{\text{type-curve}} \\
 \text{y axis :} & \quad \ln [\delta_i] = \ln \left[\frac{Q_i}{4\pi\Lambda_{ii}} \right] + \ln [E_1(u)] \quad (17)
 \end{aligned}$$

where the first right-hand side term of (17) represents the x or y type curve shift, Q_i is computed from the physical source terms using (11) and (15), and $u = r^2 S / (4Tt) = r^2 / (4\Lambda_{ii}t)$ is the dimensionless argument to E_1 . For the uncoupled electrokinetic problem, both axes are shifted in the log-log plot by the intermediate diffusivity ($1/4\Lambda_{ii}$), while the y -axis is shifted additionally by the intermediate source term (Q_i/π).

Figure 1 shows type-curve δ_i solutions for several α_D and K_D values. Figure 1b shows a zoomed-in region, where the small amount of separation between the curves for different values of K_D is visible. The solution was computed with the variable-precision library `mpmath` (Johansson et al. 2017) to confirm the dependence of the solution on numerical precision, but when terms are written correctly the solution can be computed with double precision.

The parameter range chosen has a much larger effect on δ_2 than on δ_1 . Table 1 shows $\Delta \approx \alpha_D$ and $\Lambda_{11} \approx 1$ for the α_D and K_D range chosen, while $\Lambda_{22} \approx \alpha_D$. Increasing α_D shifts the δ_i type curves both down and to the left, while decreasing K_D only shifts the curves down. The impact of changing K_D on the Q_2 value (only included in the y -shift for δ_2) is evident in Table 1, while Q_1 values do not change appreciably with K_D , because H is much larger in magnitude than G in (11) ($G \approx K_D$ and $H \approx -\alpha_D$). Table 1 shows source terms are $Q_1 \approx 2$ and $Q_2 \approx K_D/\alpha_D^2$. The physical solution for p_D and ψ_D are obtained by substituting the intermediate solutions (δ_i) into (13).

At early time in Figure 2 the electrical response (b) is larger in magnitude than the pressure response (a). The electrical response at early time ($t/r^2 < 0.01$) is surpassed at later time by the streaming potential response (ψ and p about the same magnitude). The hydraulic diffusivity controls the propagation speed in the streaming potential response; the early response due to electrical conduction from the well

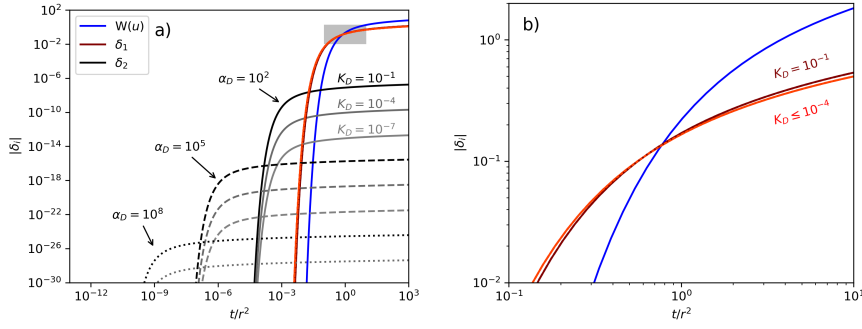


Fig. 1 a) shifted Theis solutions for δ_i for $\alpha_D = [10^2, 10^5, 10^8]$ (corresponding to solid, dashed, and dotted lines, respectively) and $K_D = [10^{-1}, 10^{-4}, 10^{-7}]$ (for dark, medium, and light colored lines, respectively). Shades of red are δ_1 (darkest red is largest K_D value), shades of black are δ_2 (black is largest K_D), and the single blue curve is un-shifted E1 type curve. Subplot b) is zoomed in to a small region in a) indicated with box in a). Different colored δ_1 curves in a) are nearly coincident.

is essentially instantaneous for $\alpha_D \gg 100$. The rate of change of the time derivative in the electrical problem has reached steady-state (i.e., the curves are largely horizontal on log-log plots) before the streaming potential response surpasses the electrical conduction from the source well.

The balance between the time scales associated with the electrical ($L_c^2/\alpha_E = b^2 C^*/\sigma_0$) and flow ($L_c^2/\alpha_H = b^2 n c \mu/k_0$) problems is captured in α_D (solid vs. dashed vs. dotted lines). The characteristic time scale for the electrical problem is much shorter than the hydrologic problem for $\alpha_D \gg 100$, which is typical. The balance between the primary (diagonal) and coupled (off-diagonal) processes is captured in K_D (darker vs. lighter colors). Larger K_D results in larger electroosmotic pressure due to an applied electrical source.

Figure 2a shows the pressure response (p) due to early-time conduction from the electrostatic source term at the well (electroosmosis). This response is sensitive to both α_D and K_D (since it is from coupling), while the electrical response (ψ in Figure 2b) at early time is not sensitive to K_D , as it arises directly from an electrical source, not a coupled source (the streaming potential response occurs later, around $t_D = 1$). The electrical response is plotted again in Figure 3 with a combination log-linear-log y-axis a) and a linear y-axis b) clearly illustrating the sign reversal. For this choice of source magnitudes (i.e., the signs of the terms in (A.19)), negative ψ responses arise from electrical conduction, while larger positive ψ responses comes from streaming potential.

For comparison, the one-dimensional radially symmetric flow problem was solved fully coupled and via eigenvalue decoupling using the finite-volume python multi-physics library `fipy` (Guyer et al. 2009). The infinite radial domain was approximated with a large radial domain ($r > 2.5$ km) with a non-uniform mesh (550 elements, starting at $\Delta r = 0.01$ m, each element growing 2% over its neighbor) and insulating/no-flow far-field boundary conditions. The dimensionless problem was solved using typical double-precision variables, using the α_D and K_D range shown

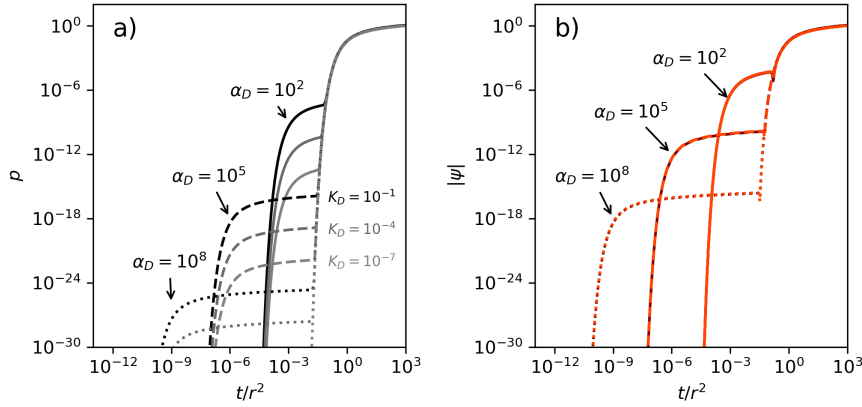


Fig. 2 Recombined physical domain solutions (a: pressure response, b: magnitude of electrical response), computed from δ_i for $\alpha_D = [10^2, 10^5, 10^8]$ (solid, dashed, and dotted lines, respectively) and $K_D = [10^{-1}, 10^{-4}, 10^{-7}]$ (for dark, medium, and light colored lines, respectively) – different colored curves representing different values of K_D in b) are nearly coincident.

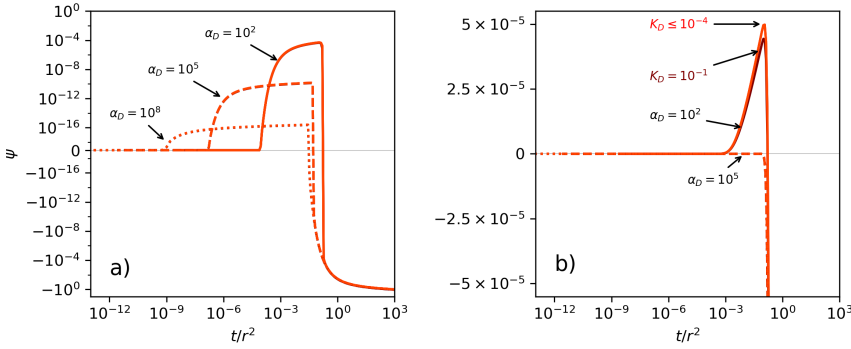


Fig. 3 Recombined physical domain electrical solution on a) linear-log y-axis scale (linear $-10^{-18} \leq y \leq 10^{-18}$ and log elsewhere) and b) linear y-axis to illustrate sign reversal of signal around $0.01 \leq t/r^2 \leq 0.1$. Line type indicates α_D value, K_D value indicated by color (curves for different K_D values are nearly coincident in a). Same curves are plotted as in Figure 2b.

in Table 1. The line source term at the origin is approximated as a 0.02 cm diameter source.

The fully coupled finite-volume problem (Figure 4a and d) produced similar results to the Theis analytical solution eigenvalue uncoupling approach (Figure 2 but using double-precision limits plotting the solution on the same scale used by the analytical type-curve method). For more direct comparison, the fipy framework was also used to solve the intermediate problems Figure 4b and e, and after recombining the two finite-volume numerical solutions were compared directly Figure 4c and f. Only for $\alpha_D > 10^{12}$ was there any difference between the two approaches, and then the

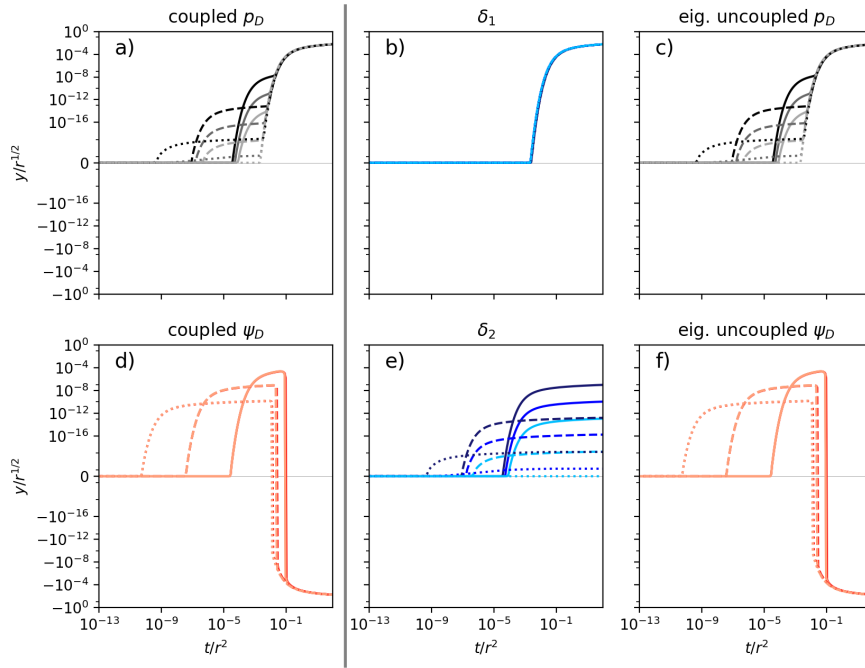


Fig. 4 Scaled finite-volume approximation of type-curve example. Subplots a) and d) show fully coupled solution, b) and e) show intermediate (δ_i) solution, c) and f) show re-combined physical solution. Solutions are for $\alpha_D = [10^2, 10^5, 10^8]$ (for solid, dashed, and dotted lines, respectively) and $K_D = [10^{-1}, 10^{-4}, 10^{-7}]$ (for dark, medium, and light colored lines, respectively).

maximum relative difference was $\approx 3 \times 10^{-4}$, occurring near the polarity reversal around $t/r^2 \approx 0.01$.

This example illustrates the eigenvalue uncoupling approach, using simplistic type-curve analysis to predict coupled physics of electrokinetics. The approach could be extended to different aquifer or pumping configurations (Maineult et al. 2008, Malama et al. 2009b;a, Malama 2014) using existing diffusion models as building blocks.

4.2 Harmonically Driven Laboratory Test

Periodically driven electrokinetics have seen some interesting laboratory applications (Pengra et al. 1999, Pengra and Wong 1999, Peng et al. 2019), including oscillatory streaming potential (Reppert et al. 2001, Tardif et al. 2011, Jouniaux and Bordes 2012, Glover et al. 2012a;b; 2020a) and electroosmosis (Reppert and Morgan 2002). In oscillatory systems, the coupling coefficient dependence on frequency becomes important (Reppert et al. 2001). This example demonstrates the eigenvalue uncoupling method for a simple-to-derive analytical solution, as an alternative to more general coupled numerical approaches.

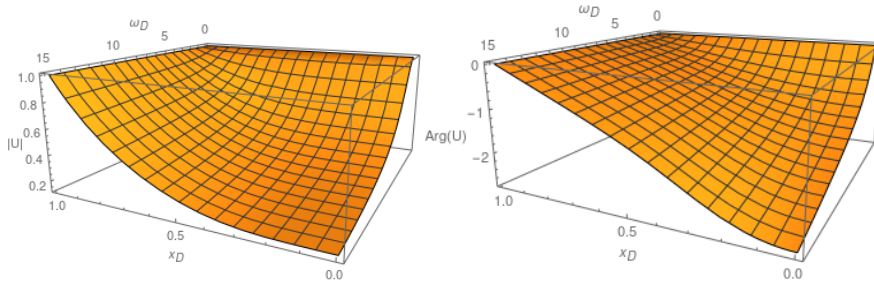


Fig. 5 Absolute value (left) and phase (right) of $U(x_D)$, showing frequency ($0 \leq \omega_D \leq 15$) and space ($0 \leq x_D \leq 1$) dependence for driven Type-I boundary condition at $x_D = 1$ and homogeneous Type-II at $x_D = 0$.

The low-frequency sinusoidal (i.e., no magnetism) driven problem is Cartesian one-dimensional, with a periodic Type-I boundary condition at $x = 1$, and a homogeneous Type-II at $x = 0$. We solve for the late-time periodic solution using separation of variables. The governing equations for flow in a one-dimensional domain are derived in Appendix B.

Figure 5 shows the real and imaginary parts of U (the complex wave amplitude). The real portion represents the amplitude while the imaginary portion shows the phase shift between the boundary condition and points inside the domain. The absolute value of U shows the largest magnitude occurs along $x_D = 1$ and $\omega_D = 0$ (left part of Figure 5), corresponding to the location of the harmonically driven boundary condition and at the low-frequency limit. The phase of U (right part of Figure 5) shows the response in the domain is in-phase with the boundary conditions at the same locations where it is largest in magnitude ($x_D = 1$ and $\omega_D = 0$), and at the far side of the domain ($x_D = 0$) and at higher frequency ($\omega_D > 10$) the solution is significantly out-of-phase with the harmonically driven boundary conditions.

Figure 6 shows the dimensionless pressure (p_D left) and electrical (ψ_D right) responses in space and time reconstructed using eigenvalue decoupling for the parameters $\omega_D = 5$, $K_D = 0.01$, and $\alpha_D = 10$. This problem has an applied sinusoidal pressure boundary condition at $x = 1$, with the response of the electrical system due to electrokinetic coupling (i.e., there is no inhomogeneous electrical source term). As given by the behavior of U in Figure 5, the left plot in Figure 6 shows the driven p_D problem is largest in magnitude along the boundary at $x_D = 1$, but different from U the right plot in Figure 6 shows the ψ_D response is zero along this same boundary. The recombination step has taken two periodic analytical solutions (δ_i) that are maximum amplitude at the boundary $x_D = 1$ and recombined them to conform to the applied boundary conditions, resulting in one periodic solution and one constant solution there. The magnitude of the oscillations in p_D decreases moving away from the driven boundary condition at $x_D = 1$, while the magnitude of the oscillations in ψ_D increase while moving away from the driven boundary condition (where they are fixed to be zero).

Figure 7 shows the analogous problem for electroosmosis (driven sinusoidal electrical boundary condition at $x_D = 1$, passive coupled pressure response). In the elec-

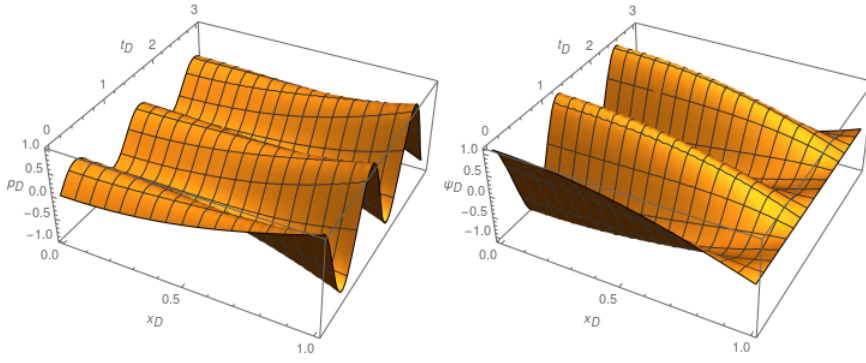


Fig. 6 Predicted dimensionless streaming potential pressure (p_D left) and electrical (ψ_D right) response for $\omega_D = 5$, $K_D = 0.01$, and $\alpha_D = 10$. Domain has driven Type-I boundary condition at $x_D = 1$, homogeneous Type-II at $x_D = 0$.

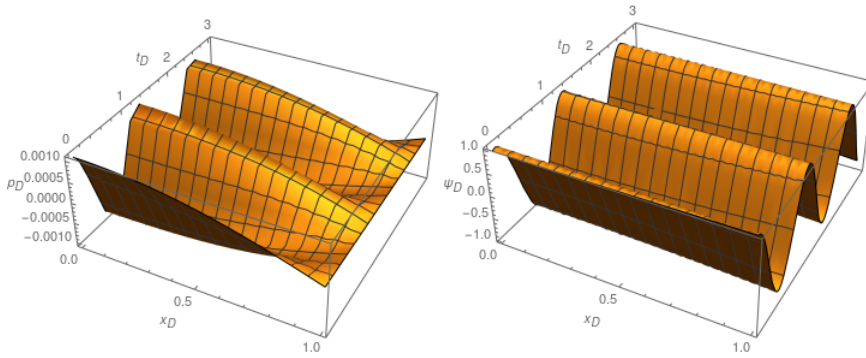


Fig. 7 Predicted dimensionless electroosmosis pressure (p_D left) and electrical (ψ_D right) response for $\omega_D = 5$, $K_D = 0.01$, and $\alpha_D = 10$. Domain has driven Type-I boundary condition at $x_D = 1$, homogeneous Type-II at $x_D = 0$.

troosmosis problem, the driven ψ_D solution is nearly constant-amplitude across the domain (due to the relatively higher electrical diffusivity), while the p_D solution amplitude increases moving away from the fixed boundary condition at $x_D = 1$, but is of relatively small overall magnitude.

This type of analytical solution (with appropriate physical dimensions and boundary conditions) could be used to fit to laboratory experimental data (e.g., Peng et al. 2019, Glover et al. 2020a;b). Using the analytical solution illustrated in the previous figures, Figure 8 illustrates solutions for three values of α_D for the electroosmosis problem (applied voltage) and the streaming potential problem (applied pressure) through time at $x_D = 0$ (left edges of plots in Figures 6 and 7). Figure 9 illustrates the same solutions plotted parametrically against one another for parameter estimation purposes, similar to analyses of laboratory data presented in Glover et al. (2020b). For the parameters chosen, these figures show the applied pressure problem (streaming potential, top) the measured pressure response does not significantly change for the range of α_D , but in the applied voltage problem (electroosmosis, bottom) the

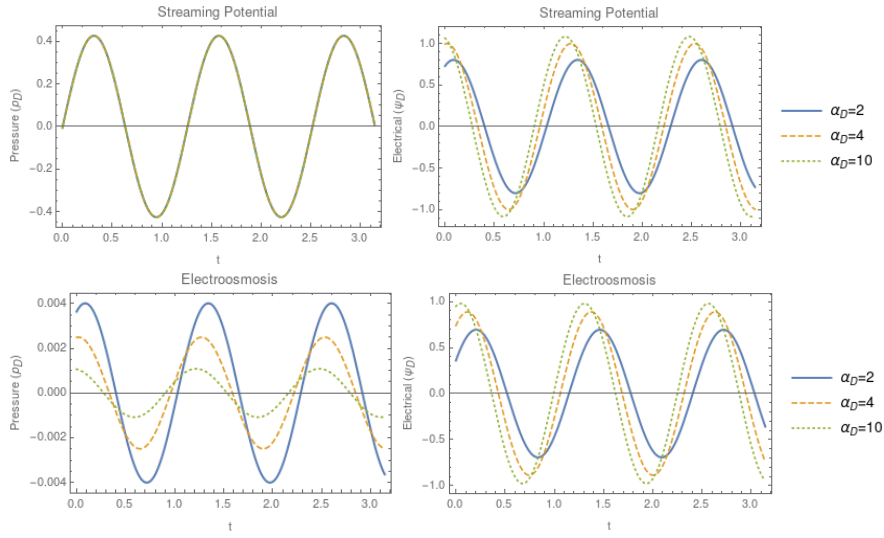


Fig. 8 Predicted pressure (left) and electrical (right) responses through time ($\omega_D = 5$, $K_D = 0.01$, $x_D = 0$) for three values of α_D . Domain has specified sinusoidal pressure (streaming potential, top) or voltage (electroosmosis, bottom) or at $x_D = 1$, no-flow and electrically insulating boundary condition at $x_D = 0$.

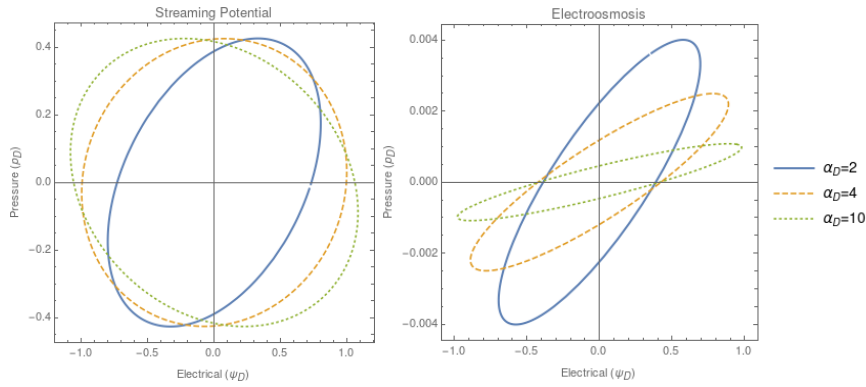


Fig. 9 Parametric plot of predicted electrical (ψ_D abscissa) and pressure (p_D ordinate) response ($\omega_D = 5$, $K_D = 0.01$, $x_D = 0$) for three values of α_D in streaming potential (left) and electroosmosis (right) problems. Same responses as previous figure, but illustrating the sinusoidal parametric form used for fitting data by Glover et al. (2020b)

measured voltage does change across the range of α_D shown here. For electroosmosis (bottom), the pressure response decrease while the voltage response increases for increasing α_D . In the electrical response for both types of tests (right), the response increases with increasing α_D . Only in the electroosmosis problem does the pressure response (left) decrease significantly with α_D (different pressure scale in two pressure plots).

5 Discussion and Method Limitations

We present an approach for exactly solving certain fully coupled electrokinetic problems, which should also be applicable to other coupled physics problems with symmetric governing equations and boundary conditions. As was shown in the examples, these problems can already be solved using fully coupled numerical models (e.g., Figure 4) or sometimes approximately using analytical solutions with only one-way coupling (Banerjee and Mitchell 1980, Shapiro and Probstein 1993, Reppert and Morgan 2002, Malama et al. 2009a;b, Malama 2014). The uncoupling approach presented here allows solving the fully coupled problem (i.e., considering both streaming potential and electroosmosis) using simpler numerical or analytical models as computational building blocks. The examples illustrate the ease at which fully coupled electrokinetic analytical solutions can be developed or re-purposed for solving coupled electrokinetic problems.

The limitations of the approach are mostly related to required symmetry. The governing equations must be symmetric (i.e., there must be analogous terms in each equation), which requires including a small transient term in the electrostatic potential equation. The boundary conditions require symmetry between the two physical problems, i.e., the electrical and hydrological equations must have compatible boundary conditions at each spatial location – they cannot have an specified voltage and specified head gradient conditions at the same location. Homogeneous boundary conditions (i.e., no change in head, no change in voltage, no-flow, or electrically insulated) are simplest, as they are unchanged between the physical and intermediate problems. The decoupling method doesn't require writing the equations in dimensionless form or permeability and electrokinetic coupling coefficients to be constant in space, but if an analytical solution is being used to solve for δ_i , dimensionless problems and homogeneous domains are more straightforward. For heterogeneous domains in numerical models, the approach requires a different set of coupling matrices computed from the flow and electrical properties (\mathbf{A} and \mathbf{S}) for each region of piecewise-constant material properties, possibly a different set of matrices at each model element.

Although some care needs to be taken when formulating the coefficients representing material properties and source terms in the intermediate problem to reduce catastrophic cancellation, the formulation of \mathbf{A} and \mathbf{S} presented here is numerically stable and can produce accurate results. While coupled numerical solutions are common and available from commercial finite-element software, analytical solutions are still useful to the hydrologist or geophysicist, since they are often dimensionless, and they do not depend on things of secondary importance to the physical problem, such as mesh resolution, domain size, and time-step size.

Table 2 Physical properties

c	compressibility	[1/Pa]
C^*	specific capacitance	[C/(m ³ · V)]
\mathbf{j}_e	current density vector	[A/m ²]
\mathbf{J}_f	Darcy flux vector	[m/s]
k_0	permeability	[m ²]
K_E	electroosmosis pressure	[Pa/V]
K_S	streaming potential	[V/Pa]
L_{12}, L_{21}	electrokinetic coupling coefficients	[A/(Pa · m)], [m ² /(V · sec)]
n	porosity	[-]
p	change in fluid pressure	[Pa]
t	time	[sec]
α_E	electrical diffusivity	[m ² /sec]
α_H	hydraulic diffusivity	[m ² /sec]
μ	water viscosity	[Pa · sec]
ψ	change in electrostatic potential	[V]
ρ	water density	[kg/m ³]
σ_0	electric conductivity	[S/m]

Table 3 Dimensionless quantities

\mathbf{A}		governing equation coefficient matrix
\mathbf{d}_D	$[\psi_D \ p_D]^T$	physical potential vector
K_D	$K_E K_S$	coupling coefficient
p_D	p/P_c	fluid pressure
r_D	r/L_c	radial distance
\mathbf{S}		eigenvector matrix
t_D	t/T_c	time
x_D	x/L_c	Cartesian distance
α_D	α_E/α_H	diffusivity ratio
$\boldsymbol{\delta}$	$[\delta_1 \ \delta_2]^T$	intermediate potential vector
$\boldsymbol{\Lambda}$		diagonal eigenvalue matrix
ψ_D	ψ/Ψ_c	electrostatic potential

6 Declarations

6.1 Funding

This work is funded by the Sandia National Laboratories Earth Science Research Foundation Laboratory-Directed Research and Development (LDRD) program.

6.2 Conflicts of interest/Competing Interests

There are no conflicts or competing interests to disclose.

6.3 Availability of Data and Materials

The Python and Mathematica scripts used to compute the solutions and make the figures are archived at Zenodo.org with the DOI 10.5281/zenodo.3979452.

Acknowledgements This paper describes objective technical results and analysis. Any subjective views or opinions expressed in the paper do not necessarily represent the views of the U.S. Department of Energy or the United States Government.

Sandia National Laboratories is a multitechnology laboratory managed and operated by National Technology & Engineering Solutions of Sandia, LLC, a wholly owned subsidiary of Honeywell International Inc., for the U.S. Department of Energy's National Nuclear Security Administration under contract DE-NA0003525.

The authors thank Tara LaForce, Paul Glover, and an anonymous reviewer for their reviews and insightful comments on the manuscript.

References

- Acar Y B, Alshawabkeh A N (1996) Electrokinetic remediation, I: Pilot-scale test with lead-spiked kaolinite. *Journal of Geotechnical Engineering* 122(3):173–185
- Acar Y B, Alshawabkeh A N, Gale R J (1993) Fundamentals of extracting species from soils by electrokinetics. *Waste Management* 13(2):141–151
- Ahmed A S, Revil A, Gross L (2019) Multiscale induced polarization tomography in hydrogeophysics: A new approach. *Advances in Water Resources* 134:103451
- Alshawabkeh A N, Sheahan T C, Wu X (2004) Coupling of electrochemical and mechanical processes in soils under DC fields. *Mechanics of Materials* 36(5–6):453–465
- Anderson E, Bai Z, Dongarra J, Greenbaum A, McKenney A, Croz J D, Hammarling S, Demmel J, Bischof C, Sorensen D (1990) LAPACK: a portable linear algebra library for high-performance computers. In *Proceedings of the 1990 ACM/IEEE Conference on Supercomputing*, IEEE Computer Society, 2–11
- Arnold M (1973) Laboratory determination of the coefficient of electro-osmotic permeability of a soil. *Géotechnique* 23(4):581–588
- Bächler D, Kohl T (2005) Coupled thermal-hydraulic-chemical modelling of enhanced geothermal systems. *Geophysical Journal International* 161(2):533–548
- Banerjee S, Mitchell J K (1980) In-situ volume-change properties by electro-osmosis—theory. *Journal of the Geotechnical Engineering Division* 106(ASCE15370)
- Banerjee S, Vitayasupakorn V (1984) Appraisal of electro-osmotic oedometer tests. *Journal of Geotechnical Engineering* 110(8):1007–1023
- Barthel R, Banzhaf S (2016) Groundwater and surface water interaction at the regional-scale—a review with focus on regional integrated models. *Water Resources Management* 30(1):1–32
- Batu V (1998) *Aquifer Hydraulics*. Wiley Interscience
- Bertolini L, Coppola L, Gastaldi M, Redaelli E (2009) Electroosmotic transport in porous construction materials and dehumidification of masonry. *Construction and Building Materials* 23(1):254–263
- Bockris J O, Reddy A K N (2002) *Modern Electrochemistry*, volume 1. Kluwer Academic, second edition
- Bruell C J, Segall B A, Walsh M T (1992) Electroosmotic removal of gasoline hydrocarbons and TCE from clay. *Journal of Environmental Engineering* 118(1):68–83
- Casagrande I L (1949) Electro-osmosis in soils. *Géotechnique* 1(3):159–177
- Coelho D, Shapiro M, Thovert J F, Adler P M (1996) Electroosmotic phenomena in porous media. *Journal of Colloid and Interface Science* 181(1):169–190
- Corapcioglu M Y (1991) Formulation of electro-chemico-osmotic processes in soils. *Transport in Porous Media* 6(4):435–444
- Gaston D, Newman C, Hansen G, Lebrun-Grandiè D (2009) MOOSE: A parallel computational framework for coupled systems of nonlinear equations. *Nuclear Engineering and Design* 239(10):1768–1778
- Glover P, Peng R, Lorinczi P, Di B (2020a) Experimental measurement of frequency-dependent permeability and streaming potential of sandstones. *Transport in Porous Media* 131(2):333–361
- Glover P W J, Peng R, Lorinczi P, Di B (2020b) Seismo-electric conversion in sandstones and shales using 2 different experimental approaches, modelling and theory. In *EGU2020*, Abstract 8454, European Geophysical Union General Assembly
- Glover P W J, Ruel J, Tardif E, Walker E (2012a) Frequency-dependent streaming potential of porous media – part 1: Experimental approaches and apparatus design. *International Journal of Geophysics* :1–15

- Glover P W J, Walker E, Ruel J, Tardif E (2012b) Frequency-dependent streaming potential of porous media – part 2: Experimental measurement of unconsolidated material. *International Journal of Geophysics* :1–17
- Gupta A, Coelho D, Adler P M (2008) Universal electro-osmosis formulae for porous media. *Journal of Colloid and Interface Science* 319(2):549–554
- Guyer J E, Wheeler D, Warren J A (2009) FiPy: Partial differential equations with Python. *Computing in Science & Engineering* 11(3):6–15
- Haines S S, Pride S R (2006) Seismoelectric numerical modeling on a grid. *Geophysics* 71(6):N57–N65
- Hammond G E, Lichtner P C, Mills R T (2014) Evaluating the performance of parallel subsurface simulators: An illustrative example with PFLOTRAN. *Water Resources Research* 50(1):208–228
- Harbaugh A W (2005) MODFLOW-2005, the US Geological Survey modular ground-water model: the ground-water flow process. US Geological Survey, Reston, VA
- Hemker C J (1984) Steady groundwater flow in leaky multiple-aquifer systems. *Journal of Hydrology* 72:355–374
- Hinnell A C, Ferrè T P A, Vrugt J A, Huisman J A, Moysey S, Rings J, Kowalsky M B (2010) Improved extraction of hydrologic information from geophysical data through coupled hydrogeophysical inversion. *Water Resources Research* 46(4)
- Hyndman D W, Harris J M, Gorelick S M (1994) Coupled seismic and tracer test inversion for aquifer property characterization. *Water Resources Research* 30(7):1965–1977
- Johansson F, Steinberg V, Kirpichev S B, Kuhlman K L, Meurer A, Čertík O, Horsen C V, Masson P, de Reyna J A, Hartmann T, Pernici M, Kagalenko M, Peterson P, Jędrzejewski-Szmek Z, Krastanov S, Warner J, Weckesser W, Buchert T, Schlömer N, Creus-Costa J, Ingold G L, Behan C, Brys A (2017) mpmath: a Python library for arbitrary-precision floating-point arithmetic
- Journiaux L, Bordes C (2012) Frequency-dependent streaming potentials: A review. *International Journal of Geophysics* :1–11
- Karniadakis G E, Beskok A, Aluru N (2005) *Microflows and Nanoflows: Fundamentals and Simulation*. Springer
- Lee T C (1999) *Applied Mathematics in Hydrogeology*. CRC Press
- Leinov E, Jackson M D (2014) Experimental measurements of the SP response to concentration and temperature gradients in sandstone with application to subsurface geophysical monitoring. *Journal of Geophysical Research: Solid Earth* 119(9):6855–6876
- Li Q, Ito K, Wu Z, Lowry C S, II S P L (2009) COMSOL Multiphysics: A novel approach to ground water modeling. *Groundwater* 47(4):480–487
- Light J C, Walker R B, Stechel E B, Schmalz T G (1979) *R*-matrix propagation methods in inelastic and reactive collisions. *Computer Physics Communications* 17(1–2):89–97
- Liu X (2013) Parallel modeling of three-dimensional variably saturated ground water flows with unstructured mesh using open source finite volume platform OpenFOAM. *Engineering Applications of Computational Fluid Mechanics* 7(2):223–238
- Lo K Y, Ho K S, Incullet I I (1991) Field test of electroosmotic strengthening of soft sensitive clay. *Canadian Geotechnical Journal* 28(1):74–83
- Lo W C, Sposito G, Majer E (2009) Analytical decoupling of poroelasticity equations for acoustic-wave propagation and attenuation in a porous medium containing two immiscible fluids. *Journal of Engineering Mathematics* 64:219–235
- Luikov A V (1975) Systems of differential equations of heat and mass transfer in capillary-porous bodies. *International Journal of Heat and Mass Transfer* 18(1):1–14
- Maas C (1986) The use of matrix differential calculus in problems of multiple-aquifer flow. *Journal of Hydrology* 88:43–67
- Maas C (1987) Groundwater flow to a well in a layered porous medium 2. nonsteady multiple-aquifer flow. *Water Resources Research* 23(8):1683–1688
- Maineult A, Strobach E, Renner J (2008) Self-potential signals induced by periodic pumping tests. *Journal of Geophysical Research* 113(B1):1–12
- Malama B (2014) Theory of transient streaming potentials in coupled unconfined aquifer-unsaturated zone flow to a well. *Water Resources Research* 50(4):2921–2945
- Malama B, Kuhlman K L, Revil A (2009a) Theory of transient streaming potentials associated with axial-symmetric flow in unconfined aquifers. *Geophysical Journal International* 179(2):990–1003
- Malama B, Revil A, Kuhlman K L (2009b) A semi-analytic solution for transient streaming potentials associated with confined aquifer pumping tests. *Geophysical Journal International* 176(3):1007–1016

- Masliyeh J H, Bhattacharjee S (2006) *Electrokinetic and Colloid Transport Phenomena*. Wiley-Interscience
- Onsager L (1931a) Reciprocal relations in irreversible processes. I. *Physical Review* 37(4):405–426
- Onsager L (1931b) Reciprocal relations in irreversible processes. II. *Physical Review* 38(12):2265–2279
- Panchekha P, Sacherz-Stern A, Wilcox J R, Tatlock Z (2015) Automatically improving accuracy for floating point expressions. In 36th Annual ACM SIGPLAN Conference on Programming Language Design and Implementation, Portland, Oregon
- Peng R, Di B, Glover P W, Wei J, Lorinczi P, Ding P, Liu Z, Zhang Y, Wu M (2019) The effect of rock permeability and porosity on seismoelectric conversion: experiment and analytical modelling. *Geophysical Journal International* 219(1):328–345
- Pengra D B, Li S X, Wong P Z (1999) Determination of rock properties by low-frequency AC electrokinetics. *Journal of Geophysical Research* 104(B12):29485–29508
- Pengra D B, Wong P Z (1999) Low-frequency AC electrokinetics. *Colloids and Surfaces A: Physicochemical and Engineering Aspects* 159(2–3):283–292
- Pollock D, Cirpka O A (2012) Fully coupled hydrogeophysical inversion of a laboratory salt tracer experiment monitored by electrical resistivity tomography. *Water Resources Research* 48(1)
- Pride S (1994) Governing equations for the coupled electromagnetics and acoustics of porous media. *Physical Review B* 50(21):15678–15696
- Probstein R F (1994) *Physicochemical Hydrodynamics*. Wiley-Interscience, second edition
- Reppert P M, Morgan F D (2002) Frequency-dependent electroosmosis. *Journal of Colloid and Interface Science* 254(2):372–383
- Reppert P M, Morgan F D, Lesmes D P, Jouniaux L (2001) Frequency-dependent streaming potentials. *Journal of Colloid and Interface Science* 234(1):194–203
- Revil A (2017) Transport of water and ions in partially water-saturated porous media. part 1. constitutive equations. *Advances in Water Resources* 103:119–138
- Revil A, Gevaudan C, Lu N, Maineult A (2008) Hysteresis of the self-potential response associated with harmonic pumping tests. *Geophysical research letters* 35(16)
- Revil A, Jarani A, Sava P, Haas A (2015) *The Seismoelectric Method*. Wiley Blackwell
- Revil A, Jardani A (2013) *The Self-Potential Method*. Cambridge
- Shapiro A P, Probstein R F (1993) Removal of contaminants from saturated clay by electroosmosis. *Environmental Science and Technology* 27(2):283–291
- Soueid Ahmed A, Jardani A, Revil A, Dupont J P (2016) Joint inversion of hydraulic head and self-potential data associated with harmonic pumping tests. *Water Resources Research* 52(9):6769–6791
- Stechel E B, Walker R B, Light J C (1978) *R*-matrix solution of coupled equations for inelastic scattering. *Journal of Chemical Physics* 69(8):3518–3531
- Strang G (1988) *Linear Algebra and its Applications*. Thomson Learning, third edition
- Tardif E, Glover P W J, Ruel J (2011) Frequency-dependent streaming potential of Ottawa sand. *Journal of Geophysics Research* 116(B4):1–15
- Theis C V (1935) The relation between lowering of the piezometric surface and the rate and duration of discharge of a well using ground-water storage. *Transactions, American Geophysical Union* 16(2):519–524
- Tsang C, Barnichon J, Birkholzer J, Li X, Liu H, Sillen X (2012) Coupled thermo-hydro-mechanical processes in the near field of a high-level radioactive waste repository in clay formations. *International Journal of Rock Mechanics and Mining Sciences* 49:31–44
- Virkutyte J, Sillanpää M, Latostenmaa P (2002) Electrokinetic soil remediation – critical overview. *Science of The Total Environment* 289(1):97–121
- Wolfram Research, Inc (2019) *Mathematica*, Version 12. Champaign, IL

A Cylindrical Flow

The governing equations for coupled fluid and electrical response due to pumping an infinitesimal diameter fully penetrating well at constant volumetric flowrate are modified from (Malama et al. 2009a;b)

$$\frac{1}{\alpha_H} \frac{\partial p}{\partial t} = K_E \frac{\partial}{\partial r} \left(r \frac{\partial \psi}{\partial r} \right) + \frac{\partial}{\partial r} \left(r \frac{\partial p}{\partial r} \right), \quad \frac{1}{\alpha_E} \frac{\partial \psi}{\partial t} = \frac{\partial}{\partial r} \left(r \frac{\partial \psi}{\partial r} \right) + K_S \frac{\partial}{\partial r} \left(r \frac{\partial p}{\partial r} \right). \quad (\text{A.18})$$

The boundary and initial conditions are

$$\begin{aligned} \lim_{r \rightarrow 0} r \frac{\partial p}{\partial r} &= \frac{-Q_T \mu}{2\pi b k_0} = -2P_c & \lim_{r \rightarrow 0} r \frac{\partial \psi}{\partial r} &= 2\Psi_c \\ p(r \rightarrow \infty, t) &= 0 & \psi(r \rightarrow \infty, t) &= 0 \\ p(r, t = 0) &= 0 & \psi(r, t = 0) &= 0, \end{aligned} \quad (\text{A.19})$$

where Q_T is the specified volumetric flowrate [m^3/sec], b is the aquifer thickness [m], r is the radial-cylinder coordinate coaxial with the pumping well [m], and t is the time since pumping began [sec]. The three constraints in (A.19) specify the constant-flowrate wellbore boundary condition, the far-field no-change condition, and the homogeneous initial condition.

The governing equations, initial conditions, and boundary conditions can be re-written in dimensionless form as

$$\begin{aligned} \frac{\partial p_D}{\partial t_D} &= K_D \frac{\partial}{\partial r_D} \left(r_D \frac{\partial p_D}{\partial r_D} \right) + \frac{\partial}{\partial r_D} \left(r_D \frac{\partial \psi_D}{\partial r_D} \right) \\ \frac{1}{\alpha_D} \frac{\partial \psi_D}{\partial t_D} &= \frac{\partial}{\partial r_D} \left(r_D \frac{\partial \psi_D}{\partial r_D} \right) + \frac{\partial}{\partial r_D} \left(r_D \frac{\partial p_D}{\partial r_D} \right) \end{aligned} \quad (\text{A.20})$$

and

$$\begin{aligned} \lim_{r_D \rightarrow 0} r_D \frac{\partial p_D}{\partial r_D} &= -2 & \lim_{r_D \rightarrow 0} r_D \frac{\partial \psi_D}{\partial r_D} &= 2 \\ p_D(r_D \rightarrow \infty, t_D) &= 0 & \psi_D(r_D \rightarrow \infty, t_D) &= 0 \\ p_D(r_D, t_D = 0) &= 0 & \psi_D(r_D, t_D = 0) &= 0. \end{aligned} \quad (\text{A.21})$$

These coupled dimensionless equations are uncoupled using the approach in Section 3, resulting in the two simpler diffusion equations

$$\frac{\partial \delta_1}{\partial t_D} = \Lambda_{11} \frac{\partial}{\partial r_D} \left(r_D \frac{\partial \delta_1}{\partial r_D} \right) \quad \frac{\partial \delta_2}{\partial t_D} = \Lambda_{22} \frac{\partial}{\partial r_D} \left(r_D \frac{\partial \delta_2}{\partial r_D} \right). \quad (\text{A.22})$$

The uncoupled boundary and initial conditions are

$$\begin{aligned} \lim_{r_D \rightarrow 0} r_D \frac{\partial \delta_1}{\partial r_D} &= \frac{2}{\Delta} (H + K_D) \equiv Q_1 & \lim_{r_D \rightarrow 0} r_D \frac{\partial \delta_2}{\partial r_D} &= -\frac{2}{\Delta} (G + K_D) \equiv Q_2 \\ \delta_1(r_D \rightarrow \infty, t_D) &= 0 & \delta_2(r_D \rightarrow \infty, t_D) &= 0 \\ \delta_1(r_D, t_D = 0) &= 0 & \delta_2(r_D, t_D = 0) &= 0. \end{aligned} \quad (\text{A.23})$$

The wellbore boundary conditions for δ_1 and δ_2 are both inhomogeneous and of different magnitude (A.23), while for the physical problem the source terms are equal and opposite in sign (A.21). Homogeneous boundary and initial conditions in the physical domain remain homogeneous in the intermediate domain.

B Oscillatory Flow

The coupled equations for electrokinetic flow in a core-scale laboratory apparatus with low-frequency oscillatory boundary conditions are derived, uncoupled, and solved using an analytical solution for a periodic steady-state solution at the same frequency as the applied boundary conditions.

B.1 Governing Equations

The governing equations for coupled fluid and electroosmotic response due to applying either sinusoidal voltage (EO) or pressure (SP) at the ends of a one-dimensional column is

$$\frac{1}{\alpha_H} \frac{\partial p}{\partial t} = K_E \frac{\partial^2 \psi}{\partial x^2} + \frac{\partial^2 p}{\partial x^2}, \quad \frac{1}{\alpha_E} \frac{\partial \psi}{\partial t} = \frac{\partial^2 \psi}{\partial x^2} + K_S \frac{\partial^2 p}{\partial x^2} \quad (\text{B.24})$$

and the boundary conditions for the applied-pressure SP problem are

$$\begin{aligned} p(x=L) &= F_p \cos(\omega t) & \psi(x=L) &= 0 \\ \left. \frac{\partial p}{\partial x} \right|_{x=0} &= 0 & \left. \frac{\partial \psi}{\partial x} \right|_{x=0} &= 0 \end{aligned} \quad (\text{B.25})$$

where F_p is the applied pressure signal amplitude [Pa] and ω is the applied boundary condition frequency [1/sec]. The analogous boundary conditions for the applied-voltage EO problem are

$$\begin{aligned} p(x=L) &= 0 & \psi(x=L) &= F_\psi \cos(\omega t) \\ \left. \frac{\partial p}{\partial x} \right|_{x=0} &= 0 & \left. \frac{\partial \psi}{\partial x} \right|_{x=0} &= 0 \end{aligned} \quad (\text{B.26})$$

where F_ψ is the applied electrostatic potential signal amplitude [V]. The domain has an arbitrary initial condition, which is omitted, since it has no influence on the steady-state solution.

Using $L_c = L$, $P_c = F_p$, and $\Psi_c = F_\psi$, the governing equation can be re-written in dimensionless form as

$$\frac{\partial p_D}{\partial t_D} = K_D \frac{\partial^2 \psi_D}{\partial x_D^2} + \frac{\partial^2 p_D}{\partial x_D^2}, \quad \frac{1}{\alpha_D} \frac{\partial \psi_D}{\partial t_D} = \frac{\partial^2 \psi_D}{\partial x_D^2} + \frac{\partial^2 p_D}{\partial x_D^2} \quad (\text{B.27})$$

while the boundary conditions are re-written in dimensionless form as

$$\begin{aligned} \left. \frac{\partial p_D}{\partial x_D} \right|_{x_D=0}^{\{\text{SP,EO}\}} &= 0 & \left. \frac{\partial \psi_D}{\partial x_D} \right|_{x_D=0}^{\{\text{SP,EO}\}} &= 0 \\ p_D^{\text{SP}}(x_D=1) &= \cos(\omega_D t_D) & \psi_D^{\text{SP}}(x_D=1) &= 0 \\ p_D^{\text{EO}}(x_D=1) &= 0 & \psi_D^{\text{EO}}(x_D=1) &= \cos(\omega_D t_D) \end{aligned} \quad (\text{B.28})$$

where $\omega_D = \omega T_c$ is the dimensionless applied frequency for the SP and EO configurations.

These dimensionless equations are uncoupled using the approach in Section 3, resulting in two uncoupled diffusion problems

$$\frac{\partial \delta_1}{\partial t_D} = \Lambda_{11} \frac{\partial^2 \delta_1}{\partial x_D^2}, \quad \frac{\partial \delta_2}{\partial t_D} = \Lambda_{22} \frac{\partial^2 \delta_2}{\partial x_D^2} \quad (\text{B.29})$$

while the inhomogeneous boundary conditions are given for the uncoupled intermediate problems (in SP or EO configurations) as

$$\begin{aligned} \delta_1^{\text{SP}}(x_D=1) &= \xi_1^{\text{SP}} \cos(\omega_D t_D) & \delta_2^{\text{SP}}(x_D=1) &= \xi_2^{\text{SP}} \cos(\omega_D t_D), \\ \delta_1^{\text{EO}}(x_D=1) &= \xi_1^{\text{EO}} \cos(\omega_D t_D) & \delta_2^{\text{EO}}(x_D=1) &= \xi_2^{\text{EO}} \cos(\omega_D t_D), \end{aligned} \quad (\text{B.30})$$

where $\xi_1^{\text{SP}} = -H/\Delta$, $\xi_2^{\text{SP}} = G/\Delta$, $\xi_1^{\text{EO}} = -K_D/\Delta$, and $\xi_2^{\text{EO}} = K_D/\Delta$. The homogeneous boundary conditions are unchanged.

In the physical problem, only one of the p_D or ψ_D boundary conditions are inhomogeneous at a time, in either the SP or EO configurations (B.28). In the intermediate uncoupled problem, both have opposite sign inhomogeneous driving terms (B.30).

B.2 Oscillatory Solution

We derive an oscillatory steady-state solution, starting with a transient diffusion problem decomposed as

$$\delta_i(x_D, t_D) = \delta_{iSS}(x_D, t_D) + \delta_{iTR}(x_D, t_D), \quad (\text{B.31})$$

namely a transient exponential decay from an arbitrary initial condition and a steady-state solution with the same frequency as the boundary condition. Here we only seek δ_{iSS} ,

$$\delta_{iSS}(x_D, t_D) = \Re [U(x_D) e^{j\omega_D t_D}], \quad (\text{B.32})$$

where $j = \sqrt{-1}$, \Re is the real part, and $U(x_D)$ is the complex amplitude. The real part ($|U(x_D)|$) is amplitude and the imaginary part ($\arg[U(x_D)]$) is phase shift. First substituting (B.32) into the uncoupled governing equations (B.29) and boundary conditions (B.30), then equating real and imaginary parts leads to the following second-order ordinary differential equation for the spatial component of the harmonic steady-state behavior

$$\frac{d^2 U}{dx_D^2} - \frac{j\omega_D}{\Lambda_{ii}} U = 0, \quad \left. \frac{dU}{dx_D} \right|_{x_D=0} = 0 \quad U(x_D = 1) = \xi_i^{\{\text{SP,EO}\}}. \quad (\text{B.33})$$

The solution to this ordinary differential equation and boundary conditions is the exponential pair

$$U_i(x_D) = c_1 e^{\zeta_i x_D} + c_2 e^{-\zeta_i x_D}, \quad (\text{B.34})$$

where $\zeta_i = \sqrt{j\omega_D/\Lambda_{ii}}$ and (c_1, c_2) are determined from the applied boundary conditions. Substituting (B.34) into the boundary conditions (B.33) and solving for (c_1, c_2) results in the steady-state solution

$$\delta_{iSS}^{\{\text{SP,EO}\}}(x_D, t_D) = \Re \left\{ \xi_i^{\{\text{SP,EO}\}} e^{j\omega_D t_D} \cosh(x_D \zeta_i) \operatorname{sech}(\zeta_i) \right\}. \quad (\text{B.35})$$